Disruption of axo–glial junctions causes cytoskeletal disorganization and degeneration of Purkinje neuron axons

German P. Garcia-Fresco*, Aurea D. Sousa†, Anilkumar M. Pillai†, Sheryl S. Moy‡§, Jacqueline N. Crawley‡§¶, Lino Tessarollo‖, Jeffrey L. Dupree**, and Manzoor A. Bhat*†§††‡‡

*Curriculum in Neurobiology, †Department of Cell and Molecular Physiology, ‡Department of Psychiatry, §Neurodevelopmental Disorders Research Center, ††Neuroscience Center, University of North Carolina School of Medicine, Chapel Hill, NC 27599; ¶Intramural Research Program, National Institute of Mental Health, Bethesda, MD 20892; ‖Neural Development Group, National Cancer Institute, Frederick, MD 21702-1201; and **Department of Anatomy and Neurobiology, Virginia Commonwealth University, Richmond, VA 23298

Communicated by Huda Y. Zoghbi, Baylor College of Medicine, Houston, TX, February 11, 2006 (received for review November 1, 2005)

Axo–glial junctions (AGJs) play a critical role in the organization and maintenance of molecular domains in myelinated axons. Neurexin IV/Caspr1/paranodin (NCP1) is an important player in the formation of AGJs because it recruits a paranodal complex implicated in the tethering of glial proteins to the axonal membrane and cytoskeleton. Mice deficient in either the axonal protein NCP1 or the glial ceramide galactosyltransferase (CGT) display disruptions in AGJs and severe ataxia. In this article, we correlate these two phenotypes and show that both *NCP1* and *CGT* mutants develop large swellings accompanied by cytoskeletal disorganization and degeneration in the axons of cerebellar Purkinje neurons. We also show that αII spectrin is part of the paranodal complex and that, although not properly targeted, this complex is still formed in *CGT* mutants. Together, these findings establish a physiologically relevant link between AGJs and axonal cytoskeleton and raise the possibility that some neurodegenerative disorders arise from disruption of the AGJs.

myelin | paranodes | cerebellum | ataxia

The anatomical organization of myelinated fibers into distinct domains is the basis for the saltatory mode of action potential propagation. In the axons, these molecular domains (internode, juxtaparanode, paranode, and node of Ranvier) form as a result of specific polarization driven by signaling between the myelinating glial cells and neurons that has yet to be fully understood. In the paranodal region, closely apposed axon-glial membranes form specialized cell junctions, which resemble the ladder-like invertebrate septate junctions, and are referred to as paranodal septate junctions or paranodal axo–glial junctions (AGJs) (1–4).

Three major proteins have been shown to localize to the paranodal AGJs: NCP1 (also known as Caspr1 or paranodin) and contactin (CNTN) on the axonal side and neurofascin (NF155), the 155-kDa isoform on the glial side (5–9). Although NF155 is the only known glial protein at the paranodal membrane, a number of nonparanodal glial proteins are required for proper formation, maintenance, and distribution of AGJs, as in the case of ceramide galactosyltransferase (CGT), proteolipid protein, myelin-basic protein, myelin-associated glycoprotein, 2′,3′-cyclic nucleotide 3′-phosphodiesterase, and the transcription factor Nkx6–2 (10–17).

Genetic ablation of *NCP1* and *CNTN* in mice results in the loss of AGJs and a failure to segregate Na^+ and K^+ channels at the nodes and juxtaparanodes, respectively (5, 6). Similar phenotypes were observed at the paranodes in *CGT* mutants (18, 19). *CGT* encodes an enzyme that is needed for the biosynthesis of two important myelin lipids, galactocerebroside and sulfatide (10, 18–21). Using subcellular fractionation of NF155 in detergents, Rasband and coworkers (22) proposed a model in which myelin lipids assemble in stable lipid rafts to stabilize the clustering of NF155 at the glial side of AGJs. This model is consistent with the phenotype of *CGT* mutants in which defective biosynthesis of components of the lipid rafts would lead to disruption of AGJs as raft microdomains may not be properly formed to allow clustering of NF155 at the paranodes. Recent studies have demonstrated that ablation of both glial (NF155) and neuronal (NF186) isoforms of neurofascin leads to disruption of both nodal and paranodal domains in myelinated fibers further strengthening the role of NF155 in AGJ formation (23).

Biochemical studies established that NCP1 associates with CNTN and that CNTN is essential for the delivery of NCP1 to paranodes in which both proteins form a high-molecular-weight complex (24–26). NCP1 is the only identified AGJ axonal protein that contains a cytoplasmic domain. Evidence gathered from biochemical and transgenic mice studies showed that the cytoplasmic domain of NCP1 binds to the actin-spectrin binding protein 4.1B (27, 28). There is growing realization that NCP1 mediates AGJ interactions with the axonal cytoskeleton and may participate in axon–glial signaling; however, physiological evidence to support these assumptions remains to be established.

NCP1 and *CGT* mutants display severe ataxia and motor coordination defects, features commonly associated with cerebellar dysfunction. In this article, we investigated the cerebellar structure of *NCP1* and *CGT* mutants and establish a correlation between disruption of AGJs and axonal degeneration in the cerebellum. This article points to a physiological significance of AGJs by demonstrating that axonal swellings develop when these junctions are disrupted in the Purkinje neurons.

Results

Behavioral Studies Suggest Cerebellar Deficits in *NCP1* Mutants. Our previous studies reported that *NCP1* mutant mice display a severe neurological phenotype (5). Starting at postnatal day 11 (P11), these mice display hypomotility, movement-associated tremor, severely impaired control and coordination of movement, and a wide-based gait suggestive of cerebellar defects (29, 30). To better investigate these phenotypes, we performed behavioral studies with *NCP1* mutant mice. *NCP1* mutant mice have an ataxic gait with a shuffling footprint pattern, a widened stance, and a lack of fore–hind foot correspondence (see Fig. 6, which is published as supporting information on the PNAS web site). We used an accelerating rotarod to assess the ability of the surviving 3-month-old *NCP1* mice to coordinate movement. WT littermate control mice demonstrated normal motor coordination and balance and exhib-

Conflict of interest statement: No conflicts declared.

Freely available online through the PNAS open access option.

Abbreviations: AGJs, axo–glial junctions; NCP1, Neurexin IV/Caspr1/paranodin; CNTN, contactin; CGT, ceramide galactosyltransferase; NF155, neurofascin; P*n*, postnatal day *n*; β-gal, β-galactosidase; TEM, transmission electron microscopy; SER, smooth endoplasmic reticulum; MS, multiple sclerosis.

‡‡To whom correspondence should be addressed. E-mail: manzoor_bhat@med.unc.edu.

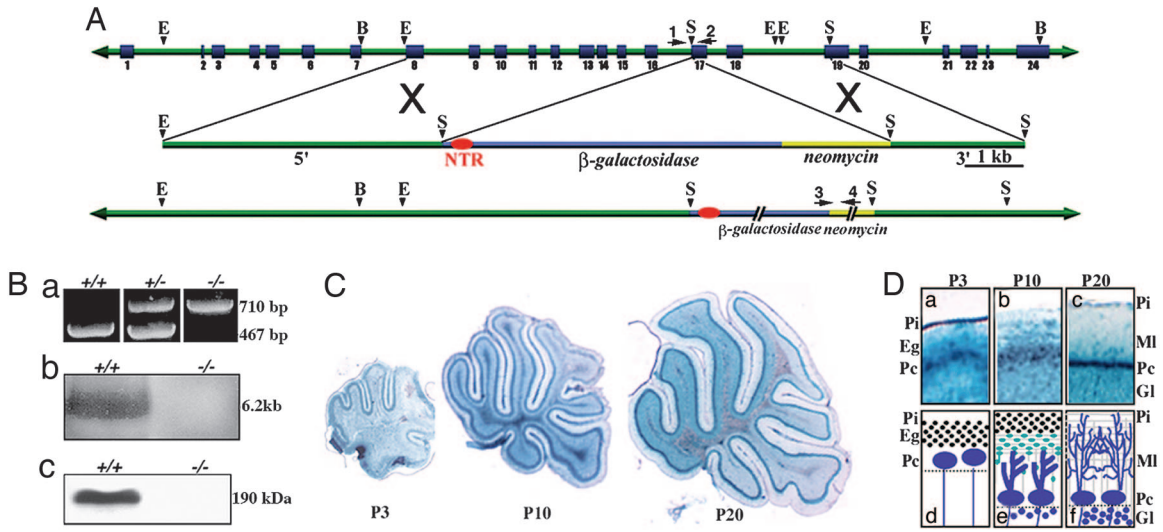

Fig. 1. Generation and analysis of *NCP1-lacZ* knockin mutants. (*A*) Restriction map of *NCP1* locus containing the entire gene and a *lacZ-neo* targeting vector. (*Ba*) Genotyping by PCR used primers (1 + 2) amplifying a 467-bp fragment for the WT and primers (3 + 4) amplifying a 710-bp fragment for the mutant allele. (*Bb*) Northern blot analysis of poly(A)$^+$ mRNA from WT and *NCP1-LacZ* mice. A 6.2-kb transcript present in the WT mice was not detected in the *NCP1-lacZ* mutants. (*Bc*) The WT animals showed a predominant protein band migrating at 190 kDa, which was not detected in the homozygous mutants. (*C*) β-gal activity seen in 30-μm sagittal sections of the cerebellum from P3, P10, and P20 *NCP1-lacZ*, with strong staining in Purkinje neurons through postnatal development. (*D*) High magnification of the cerebellar cortex of *NCP1-lacZ* animals (*a–c*). The schematic illustrates the corresponding stages of cortical development in cerebellum (*d–f*). Eg, external germinal layer; Gl, inner granular layer; Ml, molecular layer; Pc, Purkinje neuron layer; Wm, white matter.

ited significant improvement in performance over successive training trials. In contrast, the *NCP1* mice were able to remain on the accelerating rod for only a few seconds, and their performance did not improve across successive training trials. These data suggest impairment in cerebellar function.

Generation and Analysis of *NCP1-lacZ* Knockin Mice. To precisely determine which population of cells expresses *NCP1*, we generated *NCP1-lacZ* knockin mice in which transcription of *lacZ* mRNA occurs in a pattern similar to that of *NCP1* (Fig. 1*A*). Generation of heterozygous and homozygous mice was confirmed by genomic PCR analysis (Fig. 1*Ba*). Mice homozygous for the *NCP1-lacZ* allele are born at the expected Mendelian frequency from heterozygous intercrosses. These mice display an identical phenotype as that of the *NCP1* mutant mice generated previously (5). Northern blot analysis by using a cDNA probe that is downstream of the insertion site confirmed that the *NCP1-lacZ* mutation is a null mutation because no *NCP1* transcript was detected in the homozygous *NCP1-lacZ* mice compared with the WT (Fig. 1*Bb*). Western blot analysis confirmed the absence of NCP1 protein in whole-brain lysates of homozygous mutants (Fig. 1*Bc*).

To assess the expression pattern of *NCP1-lacZ*, we detected *in situ* activity of β-galactosidase (β-gal) in *NCP1-lacZ* mice at P3, P10, and P20 (Fig. 1*C*). β-gal activity was present in the Purkinje neurons and in the granular layer at all stages examined (Fig. 1 *C* and *D*). The schematic in Fig. 1*D* represents the time points analyzed according to the stage of Purkinje dendrite arborization in the molecular layer, migration of granule neurons from the external germinal layer to the granular layer, and extension of parallel fibers in the molecular layer. Note that we did not detect high β-gal activity in the molecular layer of P20 (Fig. 1*D*), which supports the assertion that the immunolocalization of NCP1 in the molecular layer at around P10 reflects the axonal compartmentalization of NCP1 in the parallel fibers. Although NCP1 localization in parallel fibers might be the major contributor for NCP1 staining in the molecular layer, we cannot rule out the possibility that NCP1 localizes to dendrites of Purkinje cells or that NCP1 is expressed at lower levels in interneurons in the molecular layer. Additional details about the developmental expression of NCP1 are presented in Fig. 7, which is published as supporting information on the PNAS web site. The gross morphology of the cerebellum was not affected by *NCP1* ablation, and neither was the timeline for landmarks in cerebellar development (see Fig. 8, which is published as supporting information on the PNAS web site).

Mutants with Disrupted AGJs Develop Axonal Swellings in Purkinje Neurons. NCP1 was localized at the paranodes in the WT cerebellar white matter (Fig. 2*A*), was absent in *NCP1* mice (Fig. 2*B*), and showed a diffuse distribution at the paranodal region in the *CGT* mice (Fig. 2*C*), consistent with refs. 5, 18, and 31. Interestingly, calbindin staining of the Purkinje neurons demonstrated large numbers of focal axonal swellings in both *NCP1* and *CGT* mutants from P10 onwards (Fig. 2 *D–I*). These swellings were observed in the myelinated regions distal to the axon initial segment (see the arrowheads in Fig. 2 *E* and *F*), and they were not observed in the Purkinje axons of WT littermates (Fig. 2*D*). At a higher resolution, Purkinje axons in *NCP1* (Fig. 2*H*) and *CGT* (Fig. 2*I*) mutant mice frequently displayed several consecutive swellings on the axon resembling beads on a string (arrowheads; compare with WT in Fig. 2*G*), some of them reaching 10–15 times the thickness of a normal myelinated axon. These data suggest that the loss of AGJs in both *NCP1* and *CGT* mutants results in the development of swellings in the Purkinje neuron axons.

Axonal Swellings Display Organelle Accumulation and Cytoskeletal Disorganization and Were Associated with Purkinje Axon Degeneration. Disruptions in axonal transport are known to cause swellings containing aggregates of cellular organelles and proteins, such as mitochondria and neurofilaments that are normally transported along the axons. To determine whether mitochondria were accumulating in these swellings, we immunostained cerebella from WT (Fig. 2*J*), *NCP1* (Fig. 2*K*), and *CGT* (Fig. 2*L*) mutants with anti-cytochrome *c* antibody, a marker for mitochondria. We found that cytochrome *c* immunoreactivity was enhanced in the swellings in *NCP1* and *CGT* axons when compared with WT axons (Fig. 2 *J–L*; arrowheads). Similar axonal swellings have also been reported

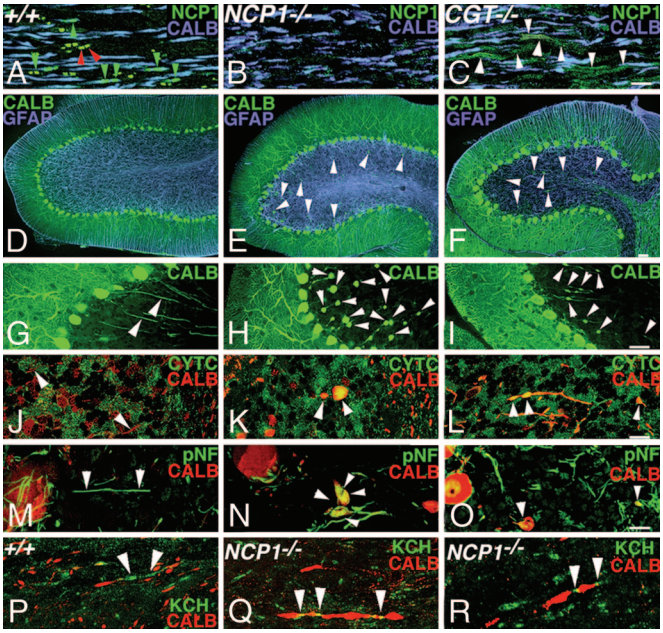

Fig. 2. Purkinje neuron axonal swellings in *NCP1* and *CGT* mutants. WT (*A*), *NCP1* (*B*), and *CGT* (*C*) mutant cerebellar white matter coimmunostained against NCP1 at paranodes (green; arrowheads) and calbindin (blue; axons). Red arrowheads point to paranodal regions of the non-Purkinje neuron axons. As expected, NCP1 is absent in *B*. In *CGT* mutants, NCP1 shows abnormal localization (compare arrowheads in *C* with *A*). Cerebellar folia from WT (*D*), *NCP1* (*E*), and *CGT* (*F*) mutants coimmunostained against calbindin (green) and GFAP (blue). The signs of axonal swellings are clearly visible (arrowheads in *E* and *F*). At a higher magnification, WT axons (*G*) show normal axons with uniform caliber, whereas *NCP1* (*H*) and *CGT* (*I*) mutant axons show a beaded appearance with axonal swellings (arrowheads). Immunostaining against the mitochondrial protein cytochrome *c* (green) shows accumulation of mitochondria in the swellings in *NCP1* (*K*; arrowheads) and *CGT* (*L*; arrowheads; compare with WT axons, *J*; arrowheads) mutants. Immunostaining against phosphorylated neurofilaments (pNF; green) in WT (*M*), *NCP1* (*N*), and *CGT* (*O*) mutants showed that the axonal swellings are enriched in pNF (arrowheads in *N* and *O*). WT axons did not show pNF accumulation in the axons (*M*; arrowheads). Immunostaining against calbindin and juxtaparanodal K^+ channels showed that small axonal swellings are flanked by paranodal K^+ channels (green; *Q* and *R*; white arrowheads). WT Purkinje axons showed normal localization of paranodal K^+ channels (*P*; green; white arrowheads). (Scale bars: *A–C*, 100 μm; *D–F*, 40 μm; *G–I*, 100 μm; *J–R*, 200 μm.)

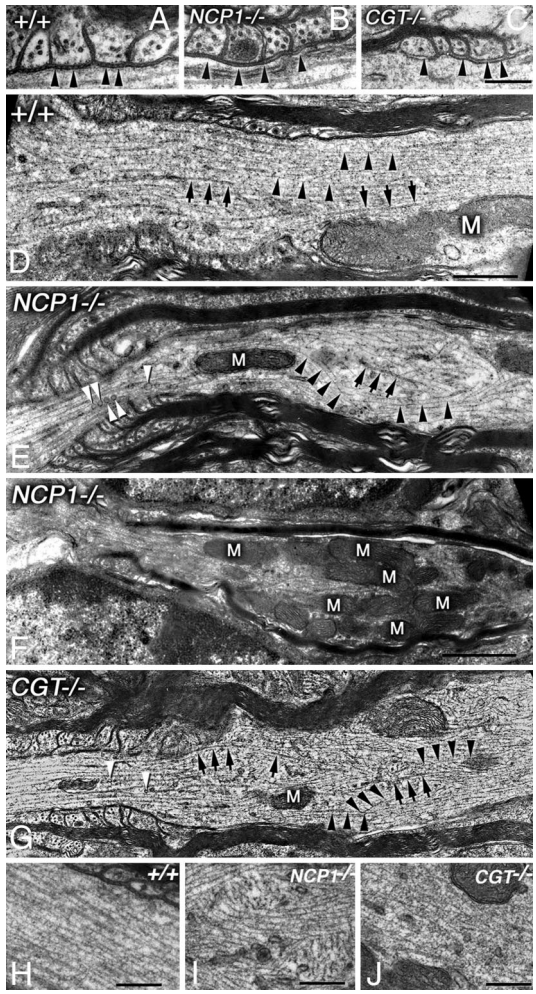

Fig. 3. Cytoskeletal abnormalities in Purkinje neuron axons in *NCP1* and *CGT* mutants. (*A*) WT myelinated axons show paranodal AGJs with clearly visible transverse septa (arrowheads). (*B*) In *NCP1* mutants, paranodal AGJ formation is abnormal and transverse septa are not formed (arrowheads). (*C*) In *CGT* mutants, AGJs fail to form, and no transverse septa are visible (arrowheads). (*D*) WT axons display a highly ordered distribution of microtubules (arrows) and neurofilaments (arrowheads) in the paranodal region. (*E*) Paranodal region from *NCP1* mutants show axonal cytoskeletal elements, neurofilaments, and microtubules, losing their ordered distribution. Several vesicles are visible along the microtubules (white arrowheads). (*F*) *NCP1* mutant axon showing abnormal accumulation of mitochondria (M) in the paranodal/juxtaparanodal region. (*G*) Paranodal region of a *CGT* mutant axon also displays disorganization of both microtubules (arrows) and neurofilaments (arrowheads). High magnification of the paranodal region shows clear disorganization of microtubular array in *NCP1* (*I*) and *CGT* (*J*) mutants compared with the WT (*H*). (Scale bars: *A–C*, 0.25 μm; *D–G*, 0.5 μm.)

in *PLP* mutants in which the accumulation of mitochondria was attributed to impairment in fast axonal transport and associated with the accumulation of phosphorylated neurofilaments (32). We therefore determined the distribution of phosphorylated neurofilaments in *NCP1* and *CGT* mutant Purkinje axons. As shown in Fig. 2 *M–O* (arrowheads), the axonal swellings in *NCP1* and *CGT* mutants also accumulated phosphorylated neurofilaments, suggesting that axonal transport was impaired in *NCP1* and *CGT* mutant axons. Interestingly, costaining by using markers for Purkinje axonal swellings (anti-calbindin) and juxtaparanodes (anti-$K_v1.1$) indicated that the juxtaparanodes in *NCP1* mutants flank small, and probably nascent, axonal swellings close to the white matter (Fig. 2 *Q–R*), which present a much more irregular diameter when compared with the WT (Fig. 2*P*). We did not detect clustering of $K_v1.1$ flanking large swellings, an indication that large swelling sizes were accompanied by diffusion of the juxtaparanodal K^+ channels.

To investigate the ultrastructure of these swellings, we performed transmission electron microscopy (TEM) of longitudinal sections of the Purkinje axons. Consistent with previous work, our TEM data show that axons from WT mice displayed transverse septa, which link the paranodal myelin loops with axolemma (Fig. 3*A*; arrowheads). In both the *NCP1* and *CGT* mutant mice, paranodal transverse septa were absent (Fig. 3 *B* and *C*; arrowheads) (5, 31). At the swellings, the *NCP1* and *CGT* mutant axons displayed severely disorganized and misoriented microtubules (arrows) and neurofilaments (arrowheads) (Fig. 3 *E* and *G*) in contrast to those of the WT axons in which these cytoskeletal elements were arranged in parallel arrays (Fig. 3*D*). This disorganization was particularly obvious at higher magnifications (Fig. 3 *I* and *J*) when compared with the WT (Fig. 3*H*). Consistent with immunofluorescence (Fig. 2), we observed that mitochondria accumulated proximal to the paranodal region (Fig. 3*F*). Taken together, the ultrastructural analyses indicate that AGJ disruption in *NCP1* and *CGT* mutants resulted in disorganized cytoskeleton and abnormal organelle accumulation specifically in the proximity of the paranodal regions.

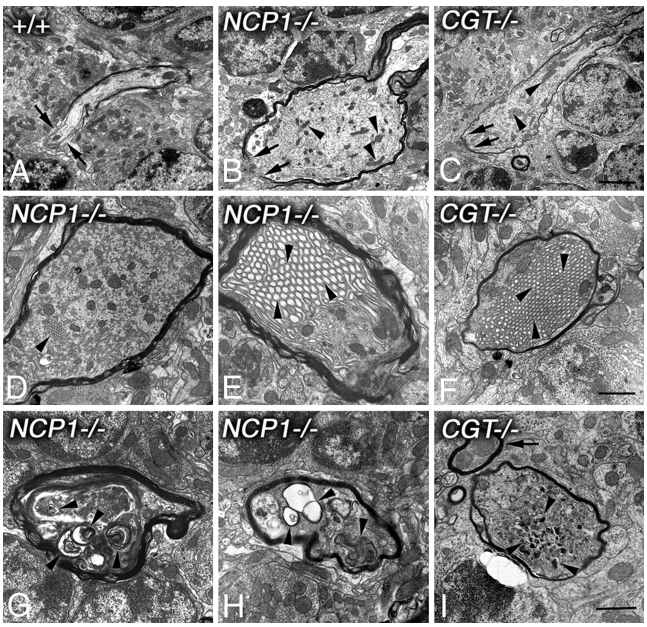

Fig. 4. Organelle accumulation and axonal degeneration in *NCP1* and *CGT* mutants. (*A*) Section of a WT axon through the paranodal region (arrows) showing normal axonal diameter and cytoskeletal organization. (*B*) An *NCP1* mutant axon shows a large swelling at the paranodal region (arrows). Note the accumulation of mitochondria (arrowheads) and cytoskeletal disorganization. (*C*) A *CGT* mutant axon also shows accumulation of mitochondria (arrowheads). Note the axon diameter disparity between WT and mutants. (*D–E*) In *NCP1* mutant axons, the most abundant components of the swellings are mitochondria and SER. Accumulation of SER results in membrane lattices, which fill most of the swellings (arrowheads). (*F*) The *CGT* mutant axonal swellings also develop SER membrane lattices as in *NCP1* mutants (arrowheads). (*G–H*) *NCP1* mutant axons in the process of degeneration showing vacuolation (arrowheads). (*I*) A *CGT* mutant axon in an early stage of degeneration displays electron dense bodies (arrowheads), which are a common feature associated with axonal decay and disorganized cytoskeleton. Arrow points to a normal myelinated axon. (Scale bars: *A–F*, 2 μm; *G–I*, 1 μm.)

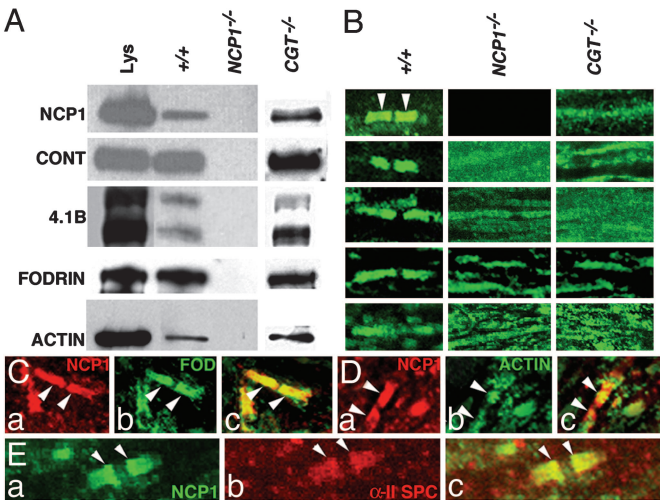

Fig. 5. AGJs at the paranodes are linked to axonal cytoskeleton. (*A*) NCP1-associated protein complex immunoprecipitated with anti-NCP1 antibodies from WT (+/+), *NCP1*, and *CGT* mutant cerebellar lysates (Lys). (*B*) Immunostaining of WT Purkinje axons by using NCP1, CNTN, 4.1B, fodrin, and actin antibodies. (*C*) Coimmunostaining of the WT Purkinje axons with NCP1 (*a*) and fodrin (*b*) antibodies shows that fodrin colocalizes with NCP1 at the AGJs (*c*; arrowheads). (*D*) Coimmunostaining with NCP1 (*a*) and actin (*b*) antibodies shows areas of overlap at the paranodal regions (*c*; arrowheads). (*E*) Coimmunostaining of the WT Purkinje axons with NCP1 (*a*) and αII spectrin-specific antibodies (*b*) shows that αII spectrin colocalizes with NCP1 at the paranodes (*c*; arrowheads).

To better visualize the ultrastructure of the axonal swellings in an effort to determine how they affect axonal diameter, we performed TEM analysis of the Purkinje axon swellings (Fig. 4). In *NCP1* (Fig. 4*B*) and *CGT* (Fig. 4*C*) mutants, we detected large axonal accumulations of organelles resulting in dramatically enlarged axon caliber compared with WT (Fig. 4*A*). Consistent with our immunofluorescence data (Fig. 2 *P* and *Q*), we found that the axonal swellings frequently form within or close to the paranodal region (see arrows in Fig. 4 *A–C*). In addition, the most frequent components of the swellings were mitochondria (arrowheads in Fig. 4 *B* and *C*) and smooth endoplasmic reticulum (SER). The accumulation of SER was so extreme that it forms a lattice filling most of the mutant axon (Fig. 4 *D–F*; arrowheads). As postnatal development continued, axonal degeneration became more prominent, as evidenced by vacuolation and fragmentation of the axonal cytoskeleton in both *NCP1* (Fig. 4 *G* and *H*; arrowheads) and *CGT* (Fig. 4*I*; arrowheads) mutants. Ultrastructural analysis of the molecular layer in *NCP1* and *CGT* mutants did not reveal any significant differences in synaptic density compared with WT (see Fig. 9, which is published as supporting information on the PNAS web site). Taken together, the immunofluorescence and TEM analyses show that disruption of AGJs lead to paranodal cytoskeletal disorganization and eventual degeneration of the Purkinje axons.

αII Spectrin Is Part of the Paranodal Complex Recruited by NCP1. In the paranodal region, the axolemma and the lateral loops of the myelin sheath maintain their closest apposition to establish the paranodal AGJs (1–4). Previous studies revealed that NCP1 recruits a complex containing axonal proteins resident at both the AGJs and cytoskeleton (2, 33, 34). The cytoskeletal disorganization observed in the *NCP1* and *CGT* mutants suggest that the molecular link between AGJs and the axonal cytoskeleton is important for local arrangement of the cytoskeletal network in Purkinje axons. Other proteins identified as part of the paranodal complex include CNTN and a brain-specific isoform of actin/spectrin-binding protein, band 4.1B (27). We therefore carried out immunoprecipitation experiments using anti-NCP1 antibodies on membrane-enriched cerebellar lysates from WT and *NCP1* and *CGT* mutants. Together with proteins reported to be part of the paranodal complex, we identified two additional cytoskeletal proteins in our immunoprecipitates: actin and the axon-specific neuronal spectrin αII spectrin (240 kDa) (Fig. 5*A*; see the +/+ column) (35, 36). Although actin is a logical candidate to be part of the complex, our results provide biochemical evidence for this assumption and strongly support the idea that the AGJs are linked to the axonal cytoskeleton. The presence of αII spectrin in NCP1 immunoprecipitates was detected by a fodrin antibody and further confirmed by αII spectrin-specific antibodies (data not shown). None of these proteins were immunoprecipitated from *NCP1* mutant lysates (Fig. 5*A*; $NCP1^{-/-}$) but were present in the *CGT* mutant immunoprecipitates (Fig. 5*A*; $CGT^{-/-}$). Taken together, these data suggest that in the absence of AGJs in *CGT* mutants NCP1 is still able to biochemically recruit the identified components of the paranodal complex.

Recruitment of a Biochemical Paranodal Complex Is Not Sufficient for AGJ Formation. To establish whether these proteins are present or enriched at the paranodes, we examined the subcellular localization of these proteins by immunofluorescence. As shown in Fig. 5*B*, NCP1 (arrowheads) and CNTN localized to the paranodes, whereas 4.1B localized to both paranodes and juxtaparanodes (Fig. 5*B* left column). The axonal αII spectrin was enriched at the paranodes in agreement with our biochemical observations. Immunostaining by using anti-actin antibodies, which is expressed

both by glia and axons, showed a modest enrichment at the paranodes in the WT axons (Fig. 5*B* left column). The paranodal localization of these proteins showed diffuse distribution in *NCP1* and *CGT* mutant axons and were not enriched at the paranodes except for NCP1, which is absent in *NCP1* mutants (Fig. 5*B* middle and right columns, respectively). Taken together, the biochemical experiments indicated that NCP1 links paranodal AGJs to axonal cytoskeleton through 4.1B and αII spectrin and that loss ($NCP1^{-/-}$) or mislocalization ($CGT^{-/-}$) of NCP1 resulted in the disruption of AGJs and destabilization of the axonal cytoskeleton around the paranodal region. To demonstrate that NCP1 colocalizes with fodrin/αII spectrin and actin at the paranodes, we performed double immunostaining. As shown in Fig. 5 *C* and *E* (arrowheads), NCP1 and fodrin/αII spectrin colocalized at the paranodes, indicating that fodrin/αII spectrin is enriched at the paranodal junctions. Similarly, immunostaining against NCP1 and actin showed some regions of colocalization in the paranodes (Fig. 5*D*; arrowheads), with expression of actin in the axons and the glial cells. Taken together, the biochemical and immunofluorescence data indicated that NCP1/4.1B/actin/αII spectrin form a biochemical complex, which localized to the paranodes, and that loss of NCP1 or mistargeting of the NCP1/4.1B/actin/αII spectrin complex (*CGT* mutants) resulted in a similar phenotype. We propose that disruption of the AGJs causes disorganization of the paranodal axonal cytoskeleton, which ultimately leads to development of axonal swellings and eventual degeneration of Purkinje neuron axons.

Discussion

In the present study, we analyzed two different mouse mutants, *NCP1* and *CGT*, which both display severe ataxia and motor coordination defects. We show that disruption of paranodal AGJs leads to cytoskeletal disorganization and degeneration of Purkinje neuron axons in the cerebellum. We also provide additional molecular evidence that AGJs are linked to the axonal cytoskeleton. Our data show that AGJs are essential not only for the organization of molecular domains in the myelinated axons (5) but also for the organization of the nodal/paranodal axonal cytoskeleton. Our studies thus establish an unappreciated role of AGJs in the maintenance of the cytoskeletal organization in myelinated axons.

Two Faces of AGJs: Glial and Neuronal. *NCP1* and *CGT* mutants display defective AGJs caused by very different mutations. *CGT* mice present genetic defects in glial cells, whereas the genetic defect in the *NCP1* mutants is in the neurons. NCP1 is a key component of AGJs on the axonal side, and the disruption of AGJs in *NCP1* mutants is due to the absence of this protein in the axons. In contrast to $NCP1^{-/-}$, the *CGT* mutants express normal levels of NCP1, but the localization at the AGJs is disrupted. CGT is required for the segregation of lipid microdomains for the clustering of NF155, the glial-binding partner of the axonal paranodal complex (8, 22). Most importantly, one would not expect *CGT* mutation to affect NCP1 function that is not related to AGJ formation because the absence of *CGT* is hypothesized to affect the clustering of the NF155-based glial complex, which is the binding partner for the NCP1/CNTN-based axonal complex at AGJs.

CNTN interacts in cis with NCP1 at the AGJs and is required for cell-surface expression of NCP1 (6, 25). *CNTN* mutants have striking defects in cerebellar development, including axonal swellings in Purkinje neurons. CNTN is expressed by several types of cerebellar neurons and has been proposed to play a role in mediating neurite outgrowth and neuronal interactions (37, 38). However, *CNTN* mutant mice exhibit more widespread defects that seem specific to *CNTN* mutants because we did not observe any parallel fiber orientation defects in *NCP1* and *CGT* mutants (38 and data not shown), suggesting that *CNTN* has additional functions which are independent of NCP1 and paranodal AGJs.

Axonal Swellings, Cytoskeletal Disorganization, and Axonal Degeneration. Axonal swellings are induced by neurotoxic chemicals (39), genetic ablation or expression of mutated genes in transgenic mice (32, 40), and neurodegenerative diseases such as amyotrophic lateral sclerosis, Charcot–Marie–Tooth disease, Wallerian degeneration, Alzheimer's disease and cerebrospinal ataxia (41–44). In all these situations, the development of swellings has been proposed to be a late sign of impairments in axonal transport. In Purkinje cells, axonal accumulation of SER has been proposed to correspond to a terminal stage of axonal degeneration (30). We found that *NCP1* and *CGT* mice develop nodal/paranodal swellings in Purkinje axons that contain aggregates of mitochondria, SER, and neurofilaments. We also detected a strong enrichment of phosphorylated neurofilaments in the axonal swellings in *NCP1* and *CGT* mutants. Besides its significance as an indicator of disrupted axonal transport, the phosphorylation of neurofilaments also modulates the interfilament spacing, and it is thought to be part of the signaling for myelin-dependent expansion of axonal caliber in the internodes (45). Although interactions between axons and glia are likely to regulate the axonal caliber, the mechanisms responsible for this regulation are not well understood (4, 46). Our findings raise the interesting possibility that AGJs might participate in axon–glial signaling, at least in the Purkinje neurons, to trigger stabilization and/or reorganization of axonal cytoskeleton. This idea is strengthened by our TEM data showing that Purkinje axons in *NCP1* and *CGT* mutants display disorganized arrays of microtubules and neurofilaments.

It has been shown that *NCP1* and *CGT* mice also have disrupted AGJs in the peripheral nerves (5, 19). We have not observed axonal swellings in the sciatic nerves of *NCP1* and *CGT* mutants at the age that we analyzed the animals (P25). Nevertheless, Purkinje neurons present incredibly high metabolic activity and may take shorter time to develop axonal swellings before mutants die than peripheral nerves. However, Purkinje somal loss was not evident at P25 (see Fig. 10, which is published as supporting information on the PNAS web site). Our data do not allow us to rule out the possibility of inherent differences in the cytoskeletal organization and mechanisms of axonal transport between the Purkinje and other neurons. It is also possible that peripheral nerves have an inbuilt compensatory mechanism to prevent the formation of the axonal swellings. A better understanding of the differences in the molecular architecture of the peripheral and central paranodal/nodal regions may be required to resolve some of these differences.

αII Spectrin: A Player in the Complex Recruited by NCP1 to Link AGJs to Axonal Cytoskeleton. Our biochemical studies showed that NCP1 forms a complex with actin and two actin-binding proteins: 4.1B and αII spectrin, which are members of protein families that associate with actin and transmembrane proteins to modulate the shape of cytoskeleton-linked membranes. Brain-specific αII spectrin has been reported to localize to myelinated axons in the cerebellum (36). Our data show that NCP1 recruited a protein complex on the axonal side of the paranodes, through which it links the AGJs to the axonal cytoskeleton. In *CGT* mutants, NCP1 retains the ability to recruit this complex despite its failure to organize the AGJs in these animals. The immunostaining data from *CGT* mutants raise an interesting possibility that the mere presence of NCP1 in the axons is not sufficient to establish or stabilize paranodal AGJs; rather, it is the proper localization of NCP1 at the paranodes that is critical for the normal organization of the axonal cytoskeleton at the paranodes.

AGJs and Relevance to Human Diseases. Human diseases such as multiple sclerosis (MS) are known to cause demyelination and axonal degeneration, but the mechanisms that lead to axonal degeneration remain largely unclear (47). Recent studies show that

NCP1 is diffused along the axons in MS lesions, suggesting that the aberrant location of NCP1 is an early sign of impending myelin loss in MS (48). In addition, NCP1-positive regions on some myelinated axons presented increased axonal caliber near the lesion edges (48). Although MS is a human disease, we show that two different mouse models of AGJ disruption presented axonal swellings close to the putative paranodal region and that the paranodal complex and/or its components were diffused in these axons. Our studies raise an interesting possibility that the pathogenesis resulting from various myelin disorders may actually be linked to compromised AGJs, leading to cytoskeletal disorganization, axonal neurodegeneration, and severe motor deficits.

Materials and Methods

Detailed experimental procedures are provided in *Supporting Materials and Methods*, which is published as supporting information on the PNAS web site.

Antibodies. The immunofluorescence methods have been described in ref. 5. The antibodies used were anti-NCP1 (5), anti-calbindin (Sigma), anti-GFAP (Chemicon), anti-cytochrome *c* (M. Deshmukh, University of North Carolina, Chapel Hill), anti-phospho-neurofilaments (Sternberger Monoclonals, Lutherville, MD), anti $K_v1.1$ channels (Sigma), anti-CNTN (J. Salzer, New York University, New York; and S. Harroch, the Pasteur Institute, Paris), anti-4.1B (P. Gascard, the Lawrence Berkeley National Laboratory, Berkeley, CA), anti-fodrin (R. Cheney, University of North Carolina), anti-αII spectrin (S. Goodman, University of Texas, Dallas), and anti-actin (Chemicon).

***NCP1-lacZ* Knockin Mice and β-Gal Activity.** 129Sv/Ev mouse genomic phage clones were isolated to establish a contiguous map of the *NCP1* locus. The construction of targeting vectors and analysis of the targeted embryonic stem cells to obtain *NCP1-lacZ* mice was carried out as described in ref. 5. For detection of β-gal, 30-μm sections were rinsed four to five times in PBS and stained at 37°C in dark for variable times with β-gal-staining solution [100 mM $K_3Fe(CN)_6$/5 mM $K_4Fe(CN)_6$/40 mg/ml 5-bromo-4-chloro-3-indolyl-β-D-galactopyranoside/2 mM $MgCl_2$ in PBS]. The color development was terminated by a quick wash in PBS before mounting.

TEM. Ultrastructural analysis of WT, *NCP1*, and *CGT* mutants was carried out as described in ref. 31.

We thank R. Cheney, M. Deshmukh, P. Gascard, S. Goodman, S. Harroch, and J. Salzer for reagents; S. Honigbaum and K. McNaughton for microscopy assistance; J. Anderson, H. Bellen, R. Cheney, A. Fanning, A. Gow, B. Philpot, K. Suzuki, and the Bhat laboratory members for comments and discussion. This work was supported by National Institutes of Health Grants GM63074 and CA78437 (to M.A.B.) and funds from the State of North Carolina.

1. Popko, B. (2003) *Nat. Genet.* **33,** 327–328.
2. Bhat, M. A. (2003) *Curr. Opin. Neurobiol.* **13,** 552–559.
3. Pedraza, L., Huang, J. K. & Colman, D. R. (2001) *Neuron* **30,** 335–344.
4. Salzer, J. L. (2003) *Neuron* **40,** 297–318.
5. Bhat, M. A., Rios, J. C., Lu, Y., Garcia-Fresco, G. P., Ching, W., St Martin, M., Li, J., Einheber, S., Chesler, M., Rosenbluth, J., Salzer, J. L. & Bellen, H. J. (2001) *Neuron* **30,** 369–383.
6. Boyle, M. E., Berglund, E. O., Murai, K. K., Weber, L., Peles, E. & Ranscht, B. (2001) *Neuron* **30,** 385–397.
7. Menegoz, M., Gaspar, P., Le Bert, M., Galvez, T., Burgaya, F., Palfrey, C., Ezan, P., Arnos, F. & Girault, J. A. (1997) *Neuron* **19,** 319–331.
8. Charles, P., Tait, S., Faivre-Sarrailh, C., Barbin, G., Gunn-Moore, F., Denisenko-Nehrbass, N., Guennoc, A. M., Girault, J. A., Brophy, P. J. & Lubetzki, C. (2002) *Curr. Biol.* **12,** 217–220.
9. Einheber, S., Zanazzi, G., Ching, W., Scherer, S., Milner, T. A., Peles, E. & Salzer, J. L. (1997) *J. Cell Biol.* **139,** 1495–1506.
10. Coetzee, T., Fujita, N., Dupree, J., Shi, R., Blight, A., Suzuki, K., Suzuki, K. & Popko, B. (1996) *Cell* **86,** 209–219.
11. Honke, K., Hirahara, Y., Dupree, J., Suzuki, K., Popko, B., Fukushima, K., Fukushima, J., Nagasawa, T., Yoshida, N., Wada, Y. & Taniguchi, N. (2002) *Proc. Natl. Acad. Sci. USA* **99,** 4227–4232.
12. Klugmann, M., Schwab, M. H., Puhlhofer, A., Schneider, A., Zimmermann, F., Griffiths, I. R. & Nave, K. A. (1997) *Neuron* **18,** 59–70.
13. Lappe-Siefke, C., Goebbels, S., Gravel, M., Nicksch, E., Lee, J., Braun, P. E., Griffiths, I. R. & Nave, K. A. (2003) *Nat. Genet.* **33,** 366–374.
14. Rasband, M. N., Tayler, J., Kaga, Y., Yang, Y., Lappe-Siefke, C., Nave, K. A. & Bansal, R. (2005) *Glia* **50,** 86–90.
15. Rosenbluth, J. (1981) *Brain Res.* **208,** 283–297.
16. Southwood, C., He, C., Garbern, J., Kamholz, J., Arroyo, E. & Gow, A. (2004) *J. Neurosci.* **24,** 11215–11225.
17. Trapp, B. D., Andrews, S. B., Cootauco, C. & Quarles, R. (1989) *J. Cell Biol.* **109,** 2417–2426.
18. Dupree, J. L., Girault, J. A. & Popko, B. (1999) *J. Cell Biol.* **147,** 1145–1152.
19. Marcus, J., Dupree, J. L. & Popko, B. (2002) *J. Cell Biol.* **156,** 567–577.
20. Dupree, J. L. & Popko, B. (1999) *J. Neurocytol.* **28,** 271–279.
21. Marcus, J., Honigbaum, S., Shroff, S., Honke, K., Rosenbluth, J. & Dupree, J. L. (2005) *Glia*, 10.1002/glia.20292.
22. Schafer, D. P., Bansal, R., Hedstrom, K. L., Pfeiffer, S. E. & Rasband, M. N. (2004) *J. Neurosci.* **24,** 3176–3185.
23. Sherman, D. L., Tait, S., Melrose, S., Johnson, R., Zonta, B., Court, F. A., Macklin, W. B., Meek, S., Smith, A. J., Cottrell, D. F. & Brophy, P. J. (2005) *Neuron* **48,** 737–742.
24. Peles, E., Nativ, M., Lustig, M., Grumet, M., Schilling, J., Martinez, R., Plowman, G. D. & Schlessinger, J. (1997) *EMBO J.* **16,** 978–988.
25. Faivre-Sarrailh, C., Gauthier, F., Denisenko-Nehrbass, N., Le Bivic, A., Rougon, G. & Girault, J. A. (2000) *J. Cell Biol.* **149,** 491–502.
26. Rios, J. C., Melendez-Vasquez, C. V., Einheber, S., Lustig, M., Grumet, M., Hemperly, J., Peles, E. & Salzer, J. L. (2000) *J. Neurosci.* **20,** 8354–8364.
27. Denisenko-Nehrbass, N., Oguievetskaia, K., Goutebroze, L., Galvez, T., Yamakawa, H., Ohara, O., Carnaud, M. & Girault, J. A. (2003) *Eur. J. Neurosci.* **17,** 411–416.
28. Gollan, L., Sabanay, H., Poliak, S., Berglund, E. O., Ranscht, B. & Peles, E. (2002) *J. Cell Biol.* **157,** 1247–1256.
29. Altman, J. & Bayer, S. A. (1997) *Development of the Cerebellar System: In Relation to Its Evolution, Structure and Functions* (CRC, Boco Raton, FL).
30. Palay, S. L. & Chan-Palay, V. (1974) *Cerebellar Cortex* (Springer, New York).
31. Dupree, J. L., Coetzee, T., Suzuki, K. & Popko, B. (1998) *J. Neurocytol.* **27,** 649–659.
32. Griffiths, I., Klugmann, M., Anderson, T., Yool, D., Thomson, C., Schwab, M. H., Schneider, A., Zimmermann, F., McCulloch, M., Nadon, N. & Nave, K. A. (1998) *Science* **280,** 1610–1613.
33. Girault, J. A., Oguievetskaia, K., Carnaud, M., Denisenko-Nehrbass, N. & Goutebroze, L. (2003) *Biol. Cell* **95,** 447–452.
34. Poliak, S. & Peles, E. (2003) *Nat. Rev. Neurosci.* **4,** 968–980.
35. Hirokawa, N., Cheney, R. E. & Willard, M. (1983) *Cell* **32,** 953–965.
36. Zagon, I. S., Higbee, R., Riederer, B. M. & Goodman, S. R. (1986) *J. Neurosci.* **6,** 2977–2986.
37. Faivre-Sarrailh, C. & Rougon, G. (1997) *Mol. Cell. Neurosci.* **9,** 109–115.
38. Berglund, E. O., Murai, K. K., Fredette, B., Sekerkova, G., Marturano, B., Weber, L., Mugnaini, E. & Ranscht, B. (1999) *Neuron* **24,** 739–750.
39. Valentine, W. M., Amarnath, V., Graham, D. G., Morgan, D. L. & Sills, R. C. (1997) *Toxicol. Appl. Pharmacol.* **142,** 95–105.
40. Ferreirinha, F., Quattrini, A., Pirozzi, M., Valsecchi, V., Dina, G., Broccoli, V., Auricchio, A., Piemonte, F., Tozzi, G., Gaeta, L., *et al.* (2004) *J. Clin. Invest.* **113,** 231–242.
41. Brownlees, J., Ackerley, S., Grierson, A. J., Jacobsen, N. J., Shea, K., Anderton, B. H., Leigh, P. N., Shaw, C. E. & Miller, C. C. (2002) *Hum. Mol. Genet.* **11,** 2837–2844.
42. Collard, J. F., Cote, F. & Julien, J. P. (1995) *Nature* **375,** 61–64.
43. Stokin, G. B., Lillo, C., Falzone, T. L., Brusch, R. G., Rockenstein, E., Mount, S. L., Raman, R., Davies, P., Masliah, E., Williams, D. S. & Goldstein, L. S. (2005) *Science* **307,** 1282–1288.
44. Zoghbi, H. Y. & Orr, H. T. (2004) *Molecular and Metabolic Bases of the Inherited Disease* (McGraw–Hill, New York).
45. Garcia, M. L., Lobsiger, C. S., Shah, S. B., Deerinck, T. J., Crum, J., Young, D., Ward, C. M., Crawford, T. O., Gotow, T., Uchiyama, Y., *et al.* (2003) *J. Cell Biol.* **163,** 1011–1020.
46. Cleveland, D. W. (1996) *Cell* **84,** 663–666.
47. Bjartmar, C., Wujek, J. R. & Trapp, B. D. (2003) *J. Neurol. Sci.* **206,** 161–171.
48. Wolswijk, G. & Balesar, R. (2003) *Brain* **126,** 1638–1649.